Original Research

Preparation and Characterization of ZnO-Ag_2O Nanostructured Films: Studying the Effect of pH on the Structure, Optical Properties, and Photocatalytic Activity

Bakr Ali Karim, N. K. Hassan*

Department of Physics, College of Education for pure Sciences, Tikrit University, 34001, Tikrit, Iraq.

* Correspondence: nadimkh4@tu.edu.iq

Received: December 14, 2025; Accepted: April 20, 2026

Abstract: To examine the impact of preparation medium pH on structural, optical, and photocatalytic capabilities, ZnO-Ag_2O hybrid nanostructured films were created using a solution-spray-deposition technique. XRD, SEM, EDX, UV-Vis absorbance, and transmittance spectroscopy were used to assess samples prepared at pH 7.5 and 9.5. Methylene Blue dye degradation under visible light was used to measure photocatalytic activity. The findings showed that the pH had a major impact on the films' efficiency and shape. In 60 minutes, the sample prepared at pH 9.5 exhibited better photocatalytic activity, achieving a removal efficiency of 32.1% compared with 24.5% for the sample prepared at pH 7.5. The improved crystallinity, uniform particle distribution, and ideal band alignment are responsible for the increased activity at pH 9.5. These results emphasize the crucial role of alkaline synthesis conditions in the development of ZnO-Ag_2O nanocomposites for environmental applications.

Keywords: ZnO, Ag_2O, thin films, nanomaterials, photocatalysis, pH.

1. Introduction

A key method for tackling the twin problems of environmental contamination and the rising need for effective industrial wastewater treatment is photocatalysis [1, 2]. The nanocomposite films in this work were particularly created using the solution spray deposition technique. Spray deposition has several advantages over traditional techniques such as sol-gel or hydrothermal synthesis, including cost-effectiveness, simplicity, scalability, and the ability to produce consistent, substrate-supported films suitable for large-scale applications [3, 4]. The capacity of semiconductor-based photocatalysts to mineralize organic pollutants into innocuous compounds under sunlight has attracted considerable research in recent decades [5]. Because of its high exciton binding energy (60 meV), chemical stability, non-toxicity, and affordability, zinc oxide (ZnO) is considered a standard material among other semiconductors [6, 7]. However, there are two significant limitations to the practical application of pure ZnO. First, light absorption is restricted to the ultraviolet (UV) region, which makes up less than 5% of the solar spectrum, due to its large bandgap (~3.37 eV) [8, 9]. Second, its quantum efficiency is greatly diminished by the quick recombination of photogenerated electron-hole pairs [10]. Building heterojunctions by combining ZnO with narrow-bandgap semiconductors has been shown to be an efficient way to get around these obstacles [11]. An excellent option is silver oxide (Ag_2O), a p-type semiconductor with a narrow bandgap (~1.2 eV) [12, 13]. Compared to single or doped binary oxide systems, the formation of a p-n ZnO-Ag_2O heterojunction suppresses the recombination of electron-hole

pairs more successfully by extending the light absorption range into the visible spectrum and facilitating the spatial separation of charge carriers [14]. Despite the potential of ZnO-Ag_2O composites, the final product's morphological, structural, and optical characteristics are largely determined by synthesis parameters, especially the pH of the precursor solution [15]. The nucleation rate, crystal growth direction, and agglomeration behavior of nanoparticles are all directly affected by pH [16, 17]. Although the impact of pH on pure ZnO has been examined, nothing is known about how it specifically affects the stoichiometry and interface quality of ZnO-Ag_2O films made via spray deposition. In contrast to recent developments in ZnO-Ag_2O heterojunctions [18, 19], which often focus on intricate synthesis pathways, our work is novel in that it employs straightforward pH control to tune the p-n junction characteristics within an affordable spray deposition framework. Additionally, whereas the basic photo catalytic routes for the degradation of methylene blue are well known [10, 20], our study focuses on the pH-driven structural development. Thus, the purpose of this work is to create ZnO-Ag_2O nan composite films, examine how pH (7.5 vs. 9.5) affects their structural development, and assess their photo catalytic activity against Methylene Blue (MB) dye under visible light.

2. Experimental part

2.1. Synthesis of ZnO-Ag_2O nanocomposite films

To ensure a uniform distribution and an effective heterojunction between the two component materials, the synthesis of ZnO-Ag_2O nanocomposite films was carried out using precise, consecutive steps. To minimize random agglomeration, distinct colloidal solutions were first prepared to ensure that each nanomaterial was individually coated with the stabilizing binder, polyvinyl alcohol (PVA).

Three g of nanostructured zinc oxide (ZnO nanoparticles, Sigma-Aldrich, St. Louis, MO, USA) and 9 g of polyvinyl alcohol (PVA, MW ~89,000-98,000, Sigma-Aldrich, St. Louis, MO, USA) were dispersed in 100 mL of double-distilled water to create solution (A). Concurrently, 1 g of nanostructured silver oxide (Ag_2O nanoparticles, Sigma-Aldrich, St. Louis, MO, USA) and 3g of PVA were dissolved in 100 mL of distilled water to create Solution (B). To ensure precursor stability and complete homogeneity prior to integration, both solutions were independently magnetically stirred for 120 minutes at 40 °C using a digital hotplate stirrer.

Solution (B) was added dropwise to Solution (A) under continuous magnetic stirring for an additional 120 minutes in order to promote the production of the ZnO-Ag_2O heterojunction. The resulting mixture was then split into two equal parts, and diluted NaOH and HCl were used to alter the medium's alkalinity to pH 7.5 and pH 9.5, respectively. To maximize interdiffusion and chemical integration between the nanoparticles, these mixtures were subjected to vigorous magnetic stirring at 150 rpm for 720 minutes (12 hours). Before the deposition process, the solutions were subjected to ultrasonication (Branson Ultrasonics, Danbury, CT, USA) for 60 minutes as a final homogenization step to break up any remaining nano-aggregates. Figure 1 shows the schematic workflow for the synthesis and thermal spray deposition process. To ensure uniform film thickness, 24 spray cycles were performed on glass substrates at 200 °C, with a constant flow rate of 2 mL/min and a nozzle-to-substrate distance of 25 cm.

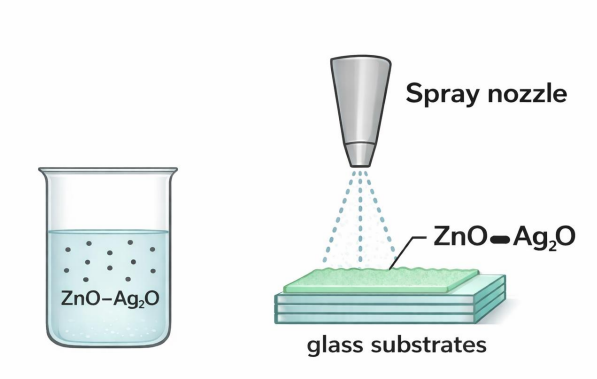

Figure 1. Schematic diagram of the solution mixing and spray deposition process onto glass substrates.

2.2. Characterization techniques and photocatalytic testing

Cu Kα radiation (λ=1.5406 Å) operating at 40 kV and 30 mA was used in X-ray diffraction (XRD-6000, Shimadzu Corp., Kyoto, Japan) to examine the crystalline structure, phase purity, and average crystallite size of the produced ZnO-Ag_2O nanocomposites. Using scanning electron microscopy (FEI Quanta 450, FEI Company, Hillsboro, OR, USA), the surface morphology, particle size distribution, and structural characteristics were investigated. To ascertain the elemental composition and mapping distribution of zinc (Zn), silver (Ag), and oxygen (O), this system was outfitted with Energy-Dispersive X-ray spectroscopy (EDX). A UV-Vis Diffuse Reflectance Spectrophotometer (UV-1800, Shimadzu Corp., Kyoto, Japan) was used to record optical characteristics, including reflectance and absorption, and to calculate the optical bandgap energy. The Tauc plot analysis method was used to determine the bandgap values. By tracking the degradation of Methylene Blue (MB) dye under visible-light irradiation, the photocatalytic activity of the ZnO-Ag_2O nanostructured films was systematically examined. The initial dye concentration was kept at 10 mg/L to provide a consistent assessment, offering the best possible balance between light penetration and substrate availability. By comparing samples prepared at pH 7.5 and 9.5, which directly affect surface morphology and active-site density, the impact of synthesis conditions was investigated. The samples were immediately exposed to visible light after the films were submerged in the dye solution, and the reaction's development was tracked at intervals of 0, 30, and 60 minutes of continuous irradiation. The films' rapid photoresponse was assessed using this direct-exposure method. To measure the reaction rate constants (k) and assess the extent to which the alkaline medium improved catalytic efficiency, the degradation kinetics were further examined using the pseudo-first-order model. Ten milligrams of powdered Methylene Blue were dissolved in 1,000 milliliters of distilled water to prepare the dye solution (10 ppm). As shown in the experimental setup in Figure 2, the substrates coated with the photocatalyst were submerged in the dye solution to guarantee surface contact. A visible light source with an intensity of 1000 W/m² was then used to irradiate the system. Using the same UV-Vis spectrophotometer, the absorbance of the solution was measured every 15 minutes for 60 minutes. The degradation efficiency (η%) was then calculated using the following formula.

$$\eta(\%)=\frac{C_0-C_t}{C_0}\times 100$$

Where C_0 represents the initial concentration of the dye (at t=0), and C_t is the concentration of the dye after irradiation time t.

OriginPro 2021 software (Version 9.8, OriginLab Corp., Northampton, MA, USA) was used for all experimental data processing, curve fitting, and kinetic computations (first-order kinetic models).

Figure 2. Experimental setup showing the ZnO-Ag_2O coated substrates immersed in Methylene Blue solution under visible light irradiation.

3. Results and discussion

3.1. Scanning electron microscopy (SEM) analysis

Depending on the precursor pH, SEM images (Figure 3) show a notable change in the films' surface morphology. The nanocomposite is made up of uniform, densely packed spherical nanoparticles with a discernible decrease in agglomeration at **pH 9.5**. This suggests that the alkaline medium has promoted balanced crystal formation and homogenous particle distribution [16].

The high concentration of OH-ions in the basic environment serves as a stabilizing factor during the nucleation process, resulting in a more regulated growth and uniform distribution of the nanoparticles [14]. On the other hand, there is noticeable particle aggregation and asymmetric distribution in the sample made at pH 7.5. This morphology is explained by the reaction's inadequate stabilization of surface forces, with a lower OH concentration causing particle clustering due to uneven electrostatic interactions [21]. It is anticipated that the effective surface area will be greater due to the more homogeneous and porous surface structure observed at pH 9.5, which offers more active sites for the adsorption of dye molecules [13].

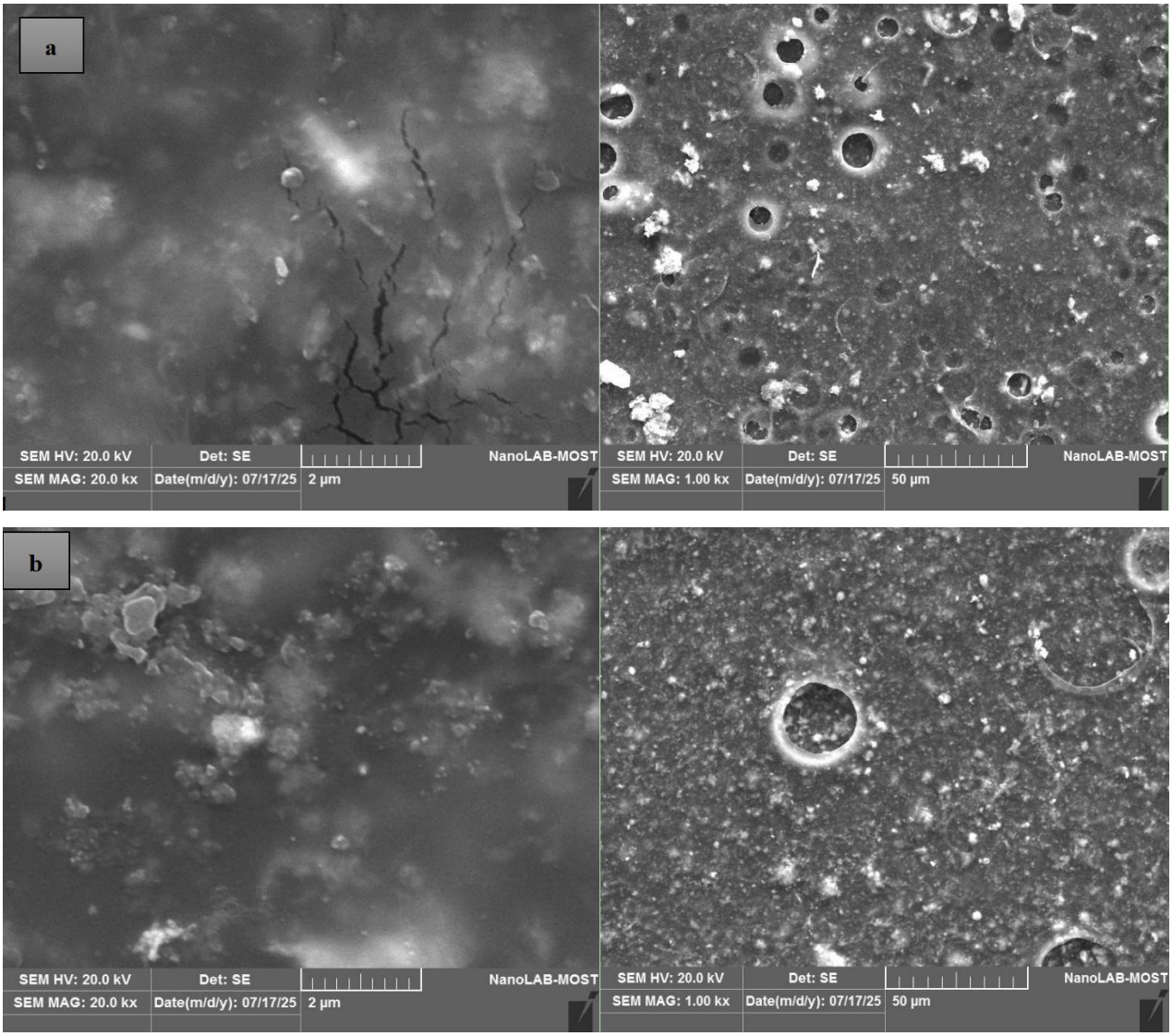

Figure 3. SEM images of the ZnO-Ag_2O nanocomposites synthesized at different precursor pH levels: (a) pH = 9.5, and (b) pH = 7.5.

3.2. Energy-dispersive x-ray spectroscopy (EDX) analysis

The purity of the ZnO-Ag_2O composite was asserted by EDX tests, which verified the existence of Zn, Ag, and O elements in the produced thin films with no discernible impurities. The elemental mapping results showed clear variations according to synthesis conditions, as shown in Figure 4. The distribution of zinc (Zn) and silver (Ag) in the sample obtained at pH 9.5 was considerably more homogenous and stoichiometrically balanced than the sample at **pH 7.5** presented in Figure 3(b), as seen in Figure 3(a).

A more regular and well-integrated hybrid nanostructure between the ZnO and Ag_2O binary phases is supported by the alkaline environment [22]**.** The creation of high-quality p-n heterojunctions depends critically on the efficient and consistent distribution of species within the matrix. These interfaces are crucial for effectively separating charge carriers and preventing photo-generated electron-hole pairs from recombining [11]. As shown in Figure 3, EDX analysis was used to confirm the purity and chemical composition of the ZnO-Ag_2O nanostructures produced. The spectra primarily show peaks that correspond to **Zn, Ag, and O**, indicating that the intended composite was formed. Additionally, the small unlabeled peaks at approximately 0.27 keV and 2.12 keV are correctly attributed to gold (Au) and carbon (C), respectively. The thin sputter-coating layer employed to improve the sample's conductivity for

high-resolution FESEM imaging is responsible for the Gold peak, whereas the Carbon signal comes from the PVA binder and conductive adhesive tape used during sample preparation [21]. The exceptional chemical purity of the produced nanostructures and the efficiency of the preparation process are confirmed by the absence of additional unknown peaks.

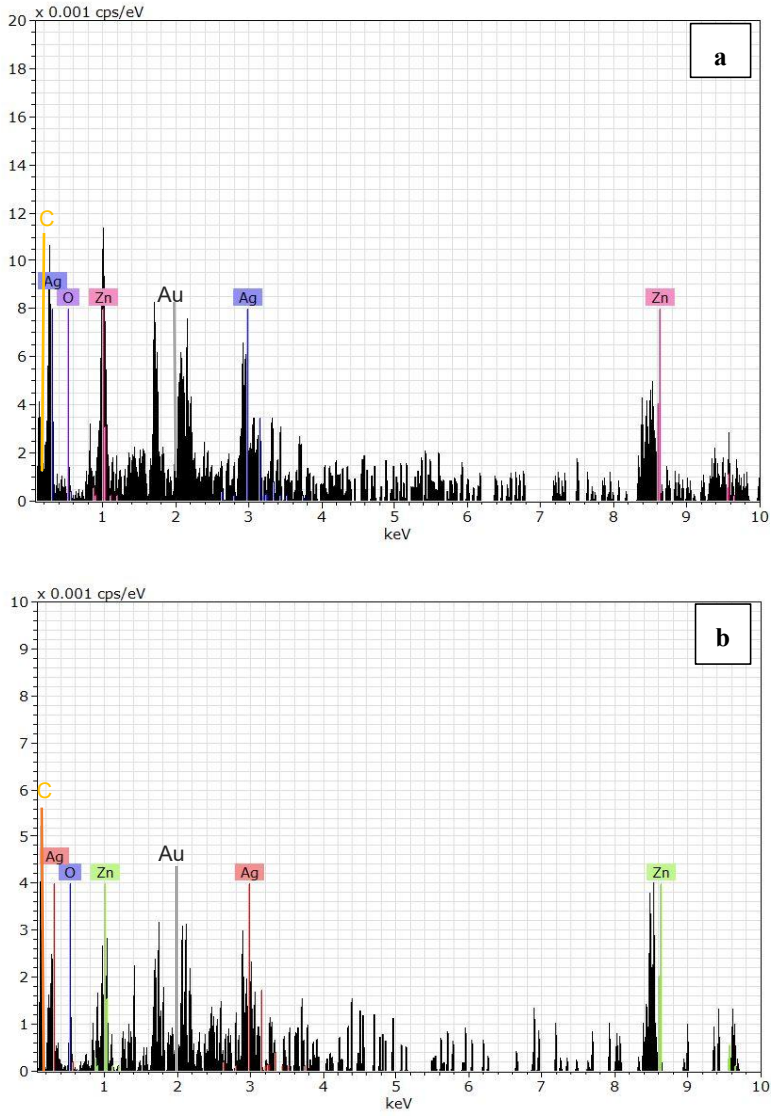

Figure 4. EDX elemental mapping distributions of the ZnO-Ag2O nanocomposites synthesized at: (a) pH = 9.5, and (b) pH = 7.5.

3.3. X-ray diffraction (XRD) analysis

The sample prepared at pH 9.5 (red line) showed noticeably sharper and more intense diffraction peaks than the sample prepared at pH 7.5 (black line), as seen in the XRD patterns displayed in Figure 5. This suggests a more uniform crystal lattice structure and increased crystallinity. The distinctive peaks denoted by (•) at 2θ values of 31.7°, 34.4°, 36.2°, 47.5°, 56.6°, and 62.8° correspond to the (100), (002), (101), (102), (110), and (103) planes, respectively, and are compatible with ZnO's hexagonal wurtzite structure (JCPDS No. 36-1451). Additionally, the (111), (200), and (220) planes of the cubic Ag_2O phase (PDF 41-1104) are represented by extra peaks denoted with (∗) at around 32.8°, 38.1°, and 54.3°. To detect all structural features, a thorough phase analysis was carried out in accordance with the fabrication of nanostructured films. The partial reduction of Ag^+ ions during chemical synthesis is responsible for the diffraction peaks

denoted by (■) at 2θ = 44.4° and 65.1°, which are attributed to the (200) and (220) planes of metallic Ag (PDF 04-0783) [23].

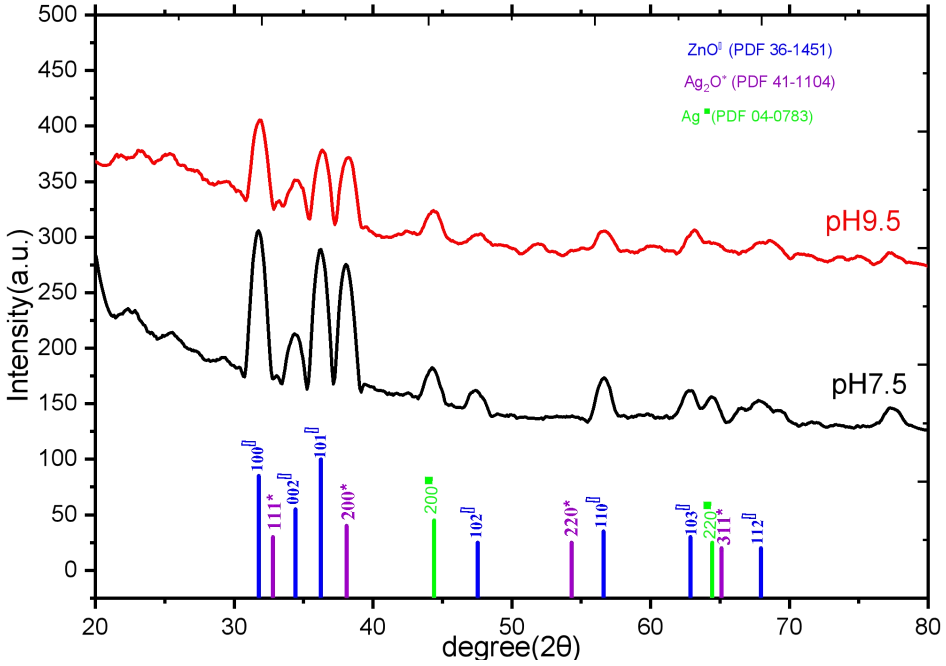

Figure 5. XRD patterns of ZnO-Ag_2O nanocomposites synthesized at pH 7.5 and pH 9.5

A systematic phase identification study was carried out by cross-referencing all recorded reflections against the JCPDS powder diffraction database to firmly verify the origin of the spectral feature near 2θ = 51°, found exclusively in the pH 9.5 diffractogram. The partial superposition of the leading wing of the Ag_2O (220) reflection centered at 2θ = 54.3° (PDF 41-1104) and the prolonged tail of the ZnO (102) Bragg reflection centered at 2θ = 47.5° (JCPDS 36-1451) is definitely responsible for this wide, low-intensity shoulder. The intensity of the Ag_2O (220) reflection is greatly increased at pH 9.5 due to the much improved crystallinity and increased phase fraction of Ag_2O, even if the individual diffraction peaks are sharper at this pH because of the decreased microstrain. An apparent shoulder in the 50°–55° region results from the amplified signal's leading baseline merging with the tail of the nearby ZnO (102) peak. The absence of any known impurity phase, such as ZnO, Ag_2O, or zinc silicate species, with a distinctive Bragg reflection at this angular point is confirmed by a thorough cross-referencing of this 2θ region against all pertinent JCPDS reference cards. The phase purity of the ZnO-Ag_2O heterojunction film is thus confirmed, as the feature at 2θ = 51° does not indicate the presence of any contaminants or foreign secondary phases.

The successful formation and phase purity of the ZnO– Ag_2O heterojunction films, in which the in situ-formed metallic Ag serves as a useful secondary phase that directly improves their optical properties and photocatalytic performance, are confirmed by the presence of these distinct diffraction peaks [12, 24]. These findings are quantitatively supported by the computed structural characteristics, which are compiled in Table 1.

Table 1. Structural parameters, grain sizes, microstrain, and dislocation densities of the ZnO-Ag_2O nanocomposites synthesized at pH 7.5 and 9.5.

Sample	Phase	Plane (hkl)	2θ (degree)	FWHM (β) (degree)	Crystallite Size (D) (nm)	d-spacing (Å)	ε ($\times 10^{-3}$)	δ ($\times 10^{14}$ line/m^2)
pH 7.5	ZnO	(101)	36.25	0.45	18.6	2.476	1.88	28.9
	Ag_2O	(111)	32.81	0.62	13.2	2.727	2.65	57.4
pH 9.5	ZnO	(101)	36.22	0.28	29.8	2.478	1.17	11.2
	Ag_2O	(111)	32.78	0.41	20.1	2.730	1.76	24.7

In particular, as the pH rose for the ZnO (101) plane, the Full Width at Half Maximum (FWHM) dropped from 0.45° to 0.28°, leading to a notable rise in the average crystallite size (D) from 18.6 nm to 29.8 nm. Similarly, crystal growth from 13.2 nm to 20.1 nm was observed in the Ag_2O phase. These findings suggest that the concentration of OH-ions in the alkaline environment encourages crystal development by facilitating the establishment of stable crystal nuclei and improving crystallization uniformity [15]. By enabling a better arrangement of atoms during nucleation, higher pH levels effectively eliminate lattice defects. On the other hand, the sample synthesized at pH 7.5 exhibits larger widths and lower peak intensities, indicating a higher density of structural flaws and weaker crystallinity due to incomplete crystal formation [25]. Using the methods presented in [26], the lattice microstrain (ε) and dislocation density (δ) were computed based on the XRD data. Microstrain and dislocation density significantly decreased as pH increased from 7.5 to 9.5, as Table 1 illustrates. The higher photocatalytic effectiveness of the nanostructured films generated at pH 9.5 is primarily due to fewer structural flaws and a significant improvement in crystalline quality. Bragg's law ($n\lambda = 2d \sin\theta$) was used to compute the interplanar separation (d-spacing). The Debye-Scherrer equation was used to estimate the average crystallite size (D):

$$D = \frac{K\lambda}{\beta cos\theta}$$

Where K is the shape factor (0.9), λ is the X-ray wavelength (1.5406 Å), β is the full width at half maximum (FWHM) in radians, and θ is the Bragg diffraction angle.

3.4. UV-visible (absorbance and transmittance) spectroscopy

The optical characteristics of the produced ZnO-Ag_2O nanocomposites were examined using spectroscopy. Figure 6 shows the absorption properties before and after photocatalytic treatment with Methylene Blue (MB) dye.

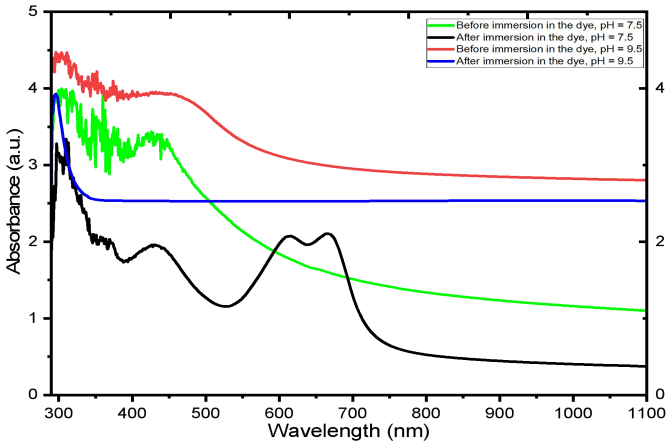

Figure 6. UV-Vis absorption spectra of ZnO-Ag_2O nanocomposites synthesized at pH 7.5 and 9.5 before and after photocatalytic degradation of Methylene Blue.

According to spectroscopic measurement, the sample prepared at pH 9.5 shows noticeably more absorption in the visible light domain than the sample made at pH 7.5. Additionally, because the produced materials are thin films, the absorption spectra were immediately recorded in transmission mode to clearly distinguish the optical signatures of Ag_2O and ZnO. The optical bandgap (E_g) values were calculated to better evaluate the impact of pH on the electronic structure. Tauc's equation $(\alpha h\nu)^n$=A($h\nu$-Eg), where n=2 for the permitted direct transition, was used to compute the bandgap [27]. As illustrated in Figure 7, this was accomplished by extending the linear part of the $(\alpha h\nu)^2$ against photon energy ($h\nu$) curves to the energy axis (Tauc plots), along with their matching absorbance spectra. For the samples generated at pH 7.5 and pH 9.5, the Tauc plots were divided into two independent graphs in order to clearly examine the electronic transitions (Figure 7a and 7b). There are two different bandgap energies in both samples. While the sample prepared at pH 9.5 exhibits bandgap values of 2.6 eV and 3.1 eV, the sample prepared at pH 7.5 exhibits bandgaps at 2.6 eV and 3.9 eV. The synergistic electrical influence of the Ag_2O integration and enhanced crystallinity is shown in this notable decrease in the primary energy gap (from 3.9 eV to 3.1 eV) [12, 28]. The pH 9.5 sample's higher photocatalytic activity and increased visible-light absorption capacity are directly supported by this progressive shift in bandgap energy.

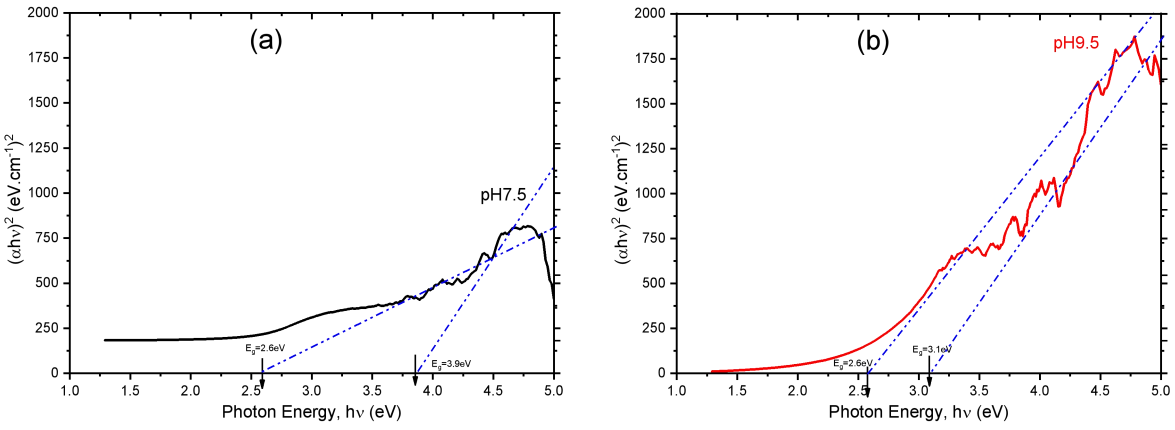

Figure 7. Optical bandgap energy evaluation (Tauc plots) of ZnO-Ag_2O nanocomposites synthesized at (a) pH 7.5 and (b) pH 9.5.

In terms of optical transparency (Figure 8a and 8b), the film prepared at pH 7.5 blocks UV light but permits a gradual increase in transmittance, reaching about 25–30% in the longer-wavelength range. On the other hand, across the entire observed spectrum (300–1100 nm), the film formed at pH 9.5 exhibits an exceptionally low, flat transmittance profile (below 10%). In contrast to the semi-transparent nature of the pH 7.5 sample, this low transmittance confirms the formation of a thick, opaque, highly light-absorbing ZnO-Ag_2O layer under more alkaline conditions [29]. The pH 9.5 film's near-zero, spectrally flat transmittance profile is a physically constant and repeatable optical response that results from three simultaneous causes. First, substantial interband absorption is provided across the UV area by the ZnO and Ag_2O phases. Second, strong plasmonic attenuation and intraband absorption across the visible and near-infrared wavelengths are attributed to the in situ-formed metallic Ag nanoparticles [23, 29]. Third and most importantly, the inverse relationship between crystallite size and surface uniformity in spray-deposited metal oxide films indicates that the much larger crystallite sizes at pH 9.5 (D = 29.8 nm for ZnO and 20.1 nm for Ag_2O, Table 1) result in a significantly higher surface roughness compared to the pH 7.5 film. Only the specular (ballistic) transmitted component is detected by the detector in a typical single-beam UV-Vis spectrophotometer arrangement; diffusely scattered light outside the acceptance angle is lost and recorded as apparent absorption. This diffuse scattering loss is significant for optically dense films with considerable surface roughness, and even over spectral regions where the material is not completely opaque, the sensor consistently records a nearly zero transmittance [29]. Spray-pyrolysis and spray-deposition nanocomposite films with similar thickness and roughness have been shown to exhibit this behavior. As a result, the measured transmittance of the pH 9.5 sample accurately reflects the film's actual light-harvesting capacity, supporting the enhanced photocatalytic performance described in Section 3.5.

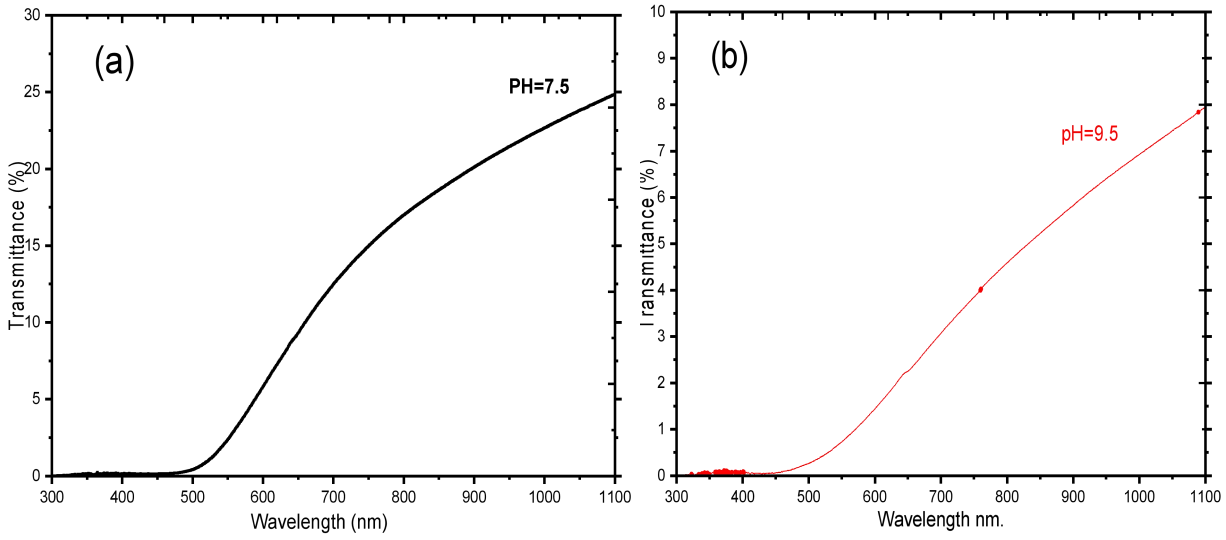

Figure 8. Transmittance spectra of the ZnO-Ag_2O nanostructured films synthesized at: (a) pH 7.5, and (b) pH 9.5, demonstrating the profound influence of deposition conditions on the films' transparency.

In terms of Methylene Blue (MB) photocatalytic degradation, the spectra of the pH 9.5 sample show complete elimination of the characteristic absorption peaks, indicating superior activity due to effective charge separation at the nanoscale interface [13].

3.5. Kinetic analysis of photocatalytic degradation

The Langmuir-Hinshelwood equation, $\ln \frac{C_0}{C_t} = k_{app}t$, as shown in Figure 9, was used to fit the experimental data to the pseudo-first-order kinetic model to quantitatively assess the reaction rate. With correlation coefficients (R^2) exceeding 0.98, the graphs show excellent linearity for both samples, demonstrating that the degradation process strictly follows first-order kinetics. The ZnO-Ag_2O (pH 9.5) sample showed the highest photocatalytic activity, with an apparent rate constant (k_{app}) of 0.0066 min^{-1} and a removal efficiency of 32.1%, according to the quantitative results shown in Table 2. The sample generated at pH 7.5, on the other hand, had a removal effectiveness of 24.5% and a reduced degradation rate (0.0048 min^{-1}). The improved surface shape and efficient spatial charge separation, which significantly decreased the electron-hole recombination rate, are responsible for the increased efficiency at pH 9.5. On the other hand, similar research indicates that aggregation in ZnO-based composites may diminish the active surface area, which is consistent with the lower activity at pH 7.5 [30]. Although the degrading efficiency (32.1%) is lower than values commonly reported for suspended powder catalysts, it is important to note that this is a feature of immobilized thin-film technology because of the lower surface-area-to-volume ratio. However, by removing the intricate post-treatment filtration procedures required in slurry systems, the immobilized film design provides a crucial practical benefit, preventing secondary contamination and simplifying catalyst recovery for industrial applications [9].

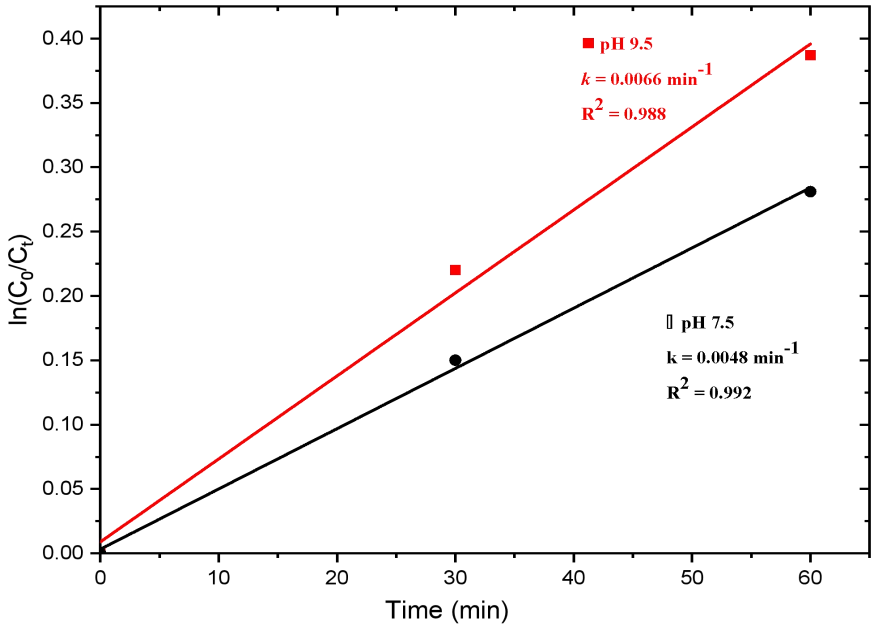

Figure 9. Linear fit of pseudo-first-order kinetics for the photocatalytic degradation of Methylene Blue over ZnO-Ag_2O nanocomposites prepared at pH 9.5 and 7.5.

Table 2. Kinetic parameters and degradation efficiency of Methylene Blue dye using ZnO-Ag_2O nanocomposites.

Sample	pH Condition	Rate Constant kapp (min−1)	Correlation Coefficient (R2)	Removal Efficiency (%)
ZnO-Ag_2O	9.5	0.0066	0.988	32.1
ZnO-Ag_2O	7.5	0.0048	0.992	24.5

3.6. Proposed photocatalytic mechanism

As schematically shown in Figure 10, a charge-transfer mechanism based on band-structure alignment is proposed to explain the improved performance. The narrow bandgap (2.6 eV) enables efficient photon absorption under visible-light irradiation, producing electron-hole pairs (e−/h+). The diagram's energy band positions indicate that ZnO's conduction band (CB) potential is roughly -0.50 eV (vs. NHE). Adsorbed oxygen molecules can be reduced to superoxide radicals (O_2^-) by this potential, which is suitably negative [31]. Concurrently, Ag_2O 's valence band (VB) potential is sufficiently positive to enable hole migration. These holes then combine with water molecules or OH-ions to produce hydroxyl radicals (•OH) or directly oxidize the dye molecules [32]. By encouraging the spatial separation of these carriers, the ZnO-Ag_2O heterojunction serves as a tactical interface that inhibits recombination. The MB dye molecules are attacked by these radicals, which causes them to completely mineralize into innocuous byproducts (CO_2, H_2O) [33, 34].

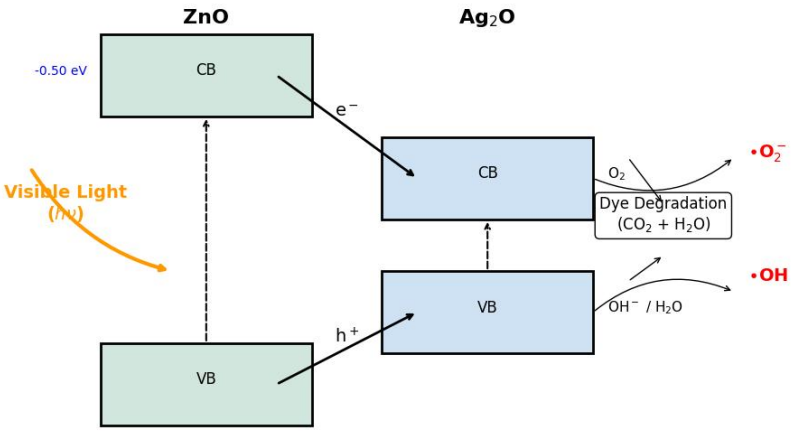

Figure 10. Schematic diagram illustrating the proposed photocatalytic mechanism and charge transfer in the ZnO-Ag_2O heterojunction.

4. Limitations of the study

There are certain limitations to consider, even though this study effectively demonstrated the increased photocatalytic activity of ZnO- Ag_2O nanocomposites synthesized at pH 9.5. Initially, Methylene Blue (MB), a cationic model pollutant, was used exclusively to assess the photocatalytic performance. A more comprehensive evaluation of the catalyst's adaptability would result from broadening the scope to include anionic dyes or complex combinations present in actual industrial effluent [4, 11]. Second, although band alignment and energy levels were used to theoretically explain the formation of reactive species -O_2 and OH), comprehensive experimental scavenger-trapping studies were not conducted in this work. These scavenging tests will be the focus of future research aimed at empirically verifying the mechanism. To guarantee the catalyst's capability for realistic industrial upscaling, assessing its long-term cyclic stability (reusability) will also be a top priority [1].

5. Conclusion

In this work, a solution-spray-deposition method was effectively used to create ZnO- Ag_2O nanocomposite films. It was found that the pH of the precursor solution significantly affected the structural and optical characteristics. The sample prepared at pH 9.5 performed much better than the sample prepared at pH 7.5 in the photocatalytic evaluation under visible-light irradiation, achieving a degradation efficiency of 32.1% and a rate constant (k) of 0.0066 min^{-1}. The modified heterojunction interface, improved crystallinity, and a notable decrease in the bandgap from 3.1 eV to 2.6 eV, which effectively inhibits photogenerated carrier recombination, are responsible for the improved performance at pH 9.5. The band-edge positions provided theoretical support for the degradation mechanism, indicating that superoxide and hydroxyl radicals are the primary active species. According to the study's findings, alkaline synthesis conditions are more effective for producing high-performance ZnO- Ag_2O photocatalytic thin films.

Funding Statement: There was no specific funding for this study. The research, writing, and publication of this work were all done without any financial assistance to the authors.

Author Contributions: Each author made an equal contribution to the work. The published version of the work has been reviewed and approved by all authors.

Availability of Data and Materials: The accompanying author can provide the data supporting the study's conclusions upon reasonable request.

Ethics Approval: Not applicable.

Conflicts of Interest: The authors declare no conflicts of interest.

References

1. Gupta, V.K.; Ali, I.; Saleh, T.A.; Nayak, A.; Agarwal, S. Chemical treatment technologies for wastewater recycling—An overview. *RSC Advances* 2012, 2(16), 6380-6388. https://doi.org/10.1039/c2ra20340e
2. Herrmann, J. M. Heterogeneous photocatalysis: Fundamentals and applications to the removal of various types of aqueous pollutants. *Catalysis Today* 1999, 53(1), 115-129. https://doi.org/10.1016/S0920-5861(99)00107-8
3. Roguai, S.; Djelloul, A. Efficient methylene blue degradation with spray-deposited ZnO, and V-doped ZnO thin films photocatalysts. *Catalysis Letters* 2025, 138, 1-38. https://doi.org/10.1007/s11144-025-02795-2
4. Altuğ, M. Charpy impact test in 3D-FDM and optimization with artificial intelligence. *Gazi Journal of Engineering Sciences* 2024, 10(1), 12-26. https://izlik.org/JA32KE52RX
5. Ong, C.B.; Ng, L.Y.; Mohammad, A.W. A review of ZnO nanoparticles as solar photocatalysts: Synthesis, mechanisms, and applications. *Renewable and Sustainable Energy Reviews* 2018, 81, 53–75. https://doi.org/10.1016/j.rser.2017.08.020
6. Kołodziejczak-Radzimska, A.; Jesionowski, T. Zinc oxide—from synthesis to application: a review. *Materials* 2014, 7(4), 2833-2881. https://doi.org/10.3390/ma7042833
7. Kumar, S.G.; Rao, K.S.R.K. Zinc oxide-based photocatalysis: tailoring surface-bulk structure and related interfacial charge carrier dynamics for better environmental applications. *RSC Advances* 2015, 5(5), 3306–3351. https://doi.org/10.1039/C4RA13299H

8. Samadi, M.; Zirak, M.; Naseri, A.; Khorasanizadeh, E.; Moshfegh, A.Z. Recent progress in doping of ZnO nanostructures for photocatalytic applications: a review. *Thin Solid Films* 2016, 605, 2–19. https://doi.org/10.1016/j.tsf.2015.12.064
9. Wu, J.; Xue, D. Progress of science and technology of ZnO as advanced material. *Science of Advanced Materials* 2011, 3(2), 127-149. https://doi.org/10.1166/sam.2011.1144
10. Lee, K.M.; Lai, C.W.; Ngai, K.S.; Juan, J.C. Recent developments of zinc oxide-based photocatalyst in water treatment technology: A review. *Water Research* 2016, 88, 428–448. https://doi.org/10.1016/j.watres.2015.09.045
11. Wang, H.; Zhang, L.; Chen, Z.; Hu, J.; Li, S.; Wang, Z.; Liu, B.; Wang, X. Semiconductor heterojunction photocatalysts: Design, construction, and photocatalytic performances. *Chemical Society Reviews* 2014, 43(15), 5234-5244. https://doi.org/10.1039/C4CS00126E
12. Ma, S.; Xue, J.; Zhou, Y.; Zhang, Z. Photochemical synthesis of ZnO-Ag_2O heterostructures with enhanced ultraviolet and visible photocatalytic activity. *Journal of Materials Chemistry A* 2014, 2(19), 7272–7280. https://doi.org/10.1039/C4TA00464G
13. Mohamed, R.M.; Ismail, A.A.; Kadi, M.W.; Alresheedi, A.S.; Mkhalid, I.A. Facile synthesis of mesoporous Ag_2O–ZnO heterojunctions for efficient promotion of visible centrifugation light photodegradation of tetracycline. *ACS Omega* 2020, 5(51), 33269–33279. https://doi.org/10.1021/acsomega.0c04969
14. Goktas, A. High-quality solution-based Co and Cu co-doped ZnO nanocrystalline thin films: Comparison of the effects of air and argon annealing environments. *Journal of Alloys and Compounds* 2018, 735, 2038-2045. https://doi.org/10.1016/j.jallcom.2017.11.391
15. Alias, S.S.; Ismail, A.B.; Mohamad, A.A. Effect of pH on ZnO nanoparticle properties synthesized by sol-gel centrifugation. *Journal of Alloys and Compounds* 2010, 499(2), 231–237. https://doi.org/10.1016/j.jallcom.2010.03.174
16. Londhe, P.U.; Chaure, N.B. Effect of pH on the properties of electrochemically prepared ZnO thin films. *Materials Science in Semiconductor Processing* 2017, 60, 5–15. https://doi.org/10.1016/j.mssp.2016.12.005
17. Wahab, R.; Ansari, S.G.; Kim, Y.S.; Seo, H.K.; Shin, H.S. The role of pH variation on the growth of zinc oxide nanostructures. *Applied Surface Science* 2009, 255(9), 4891–4896. https://doi.org/10.1016/j.apsusc.2008.12.037
18. Feng, W.; Wang, Y.; Zhang, L.; Zhang, X.; Liu, J.; Li, H. Engineering charge transfer characteristics in ZnO NRs/ Ag_2O NPs p–n heterojunctions. *Langmuir* 2024, 40(47), 24842-24853. https://doi.org/10.1021/acs.langmuir.4c02670
19. Mamba, F.B.; Ndlangamandla, S.; Mamba, G. Synergistic effect of ZnO/ Ag_2O @g-C3N4 based nanocomposites. *Heliyon* 2024, 10(11), e31109. https://doi.org/10.1016/j.heliyon.2024.e31109
    Chakrabarti, S.; Dutta, B.K. Photocatalytic degradation of model textile dyes in wastewater using ZnO as semiconductor catalyst. *Journal of Hazardous Materials* 2004, 112(3), 269–278. https://doi.org/10.1016/j.jhazmat.2004.05.013
21. Rayerfrancis, A.; Bhargav, P.B.; Ahmed, N.; Chandra, B.; Dhara, S. Effect of pH on the morphology of ZnO nanostructures and its influence on structural and optical properties. *Physica B: Condensed Matter* 2015, 457, 96–102. https://doi.org/10.1016/j.physb.2014.09.044
22. Kaur, J.; Singhal, S. Facile synthesis of ZnO and transition metal doped ZnO nanoparticles for the photocatalytic degradation of Methyl Orange. Ceramics International, 40(5), 7417-7424. https://doi.org/10.1016/j.ceramint.2013.12.088

23. Sahu, P.; Das, D. Two-step visible light photocatalytic dye degradation phenomena in Ag_2O-impregnated ZnO nanorods via growth of metallic Ag and formation of $ZnO/Ag^0/Ag_2O$ heterojunction structures. *Langmuir* 2022, 38(15), 4503-4520, 2022. https://doi.org/10.1021/acs.langmuir.1c02860
24. Hamza, B.M.; Chuah, L.S.; Purushothaman, S. Synthesis and characterization of Ag–ZnO nanocomposites. Journal of Optoelectronic and Biomedical Materials, 17(1), 35–39. https://www.chalcogen.ro/35_HamzaBM.pdf
25. Xiong, G.; Pal, U.; Serrano, J. G.; Ucer, K. B.; Williams, R. T. Photoluminescence and FTIR study of ZnO nanoparticles: The impurity and defect perspective. *Physica Status Solidi (c)* 2006, 3(10), 3577-3581. https://doi.org/10.1002/pssc.200672164
26. Fathy, N.; Fathy, S.; Ali, F.; Mousa, S. Effective sunlight photodegradation of methylene blue dye using zinc oxide doped with mono- and bi-metals of Ag and Ce. *Desalination and Water Treatment* 2024, 320, 100595. https://doi.org/10.1016/j.dwt.2024.100595
27. Tauc, J.; Grigorovici, R.; Vancu, A. Optical properties and electronic structure of amorphous germanium. *Physica Status Solidi (b)* 1966, 15(2), 627–637. https://doi.org/10.1002/pssb.19660150224
28. Zheng, Y.; Zheng, L.; Zhan, Y.; Lin, X.; Zheng, Q.; Wei, K. Ag/ZnO heterostructure nanocrystals: synthesis, characterization, and photocatalysis. *Inorganic Chemistry* 2007, 46(17), 6980–6986. https://doi.org/10.1021/ic700688f
29. Ibraheem, A.M.; Kamalakkannan, J. Sustainable scientific advancements modified Ag_2O-ZnO thin films characterization and application of photocatalytic purification of carcinogenic dye in deionizer water and contaminated sea water solutions and synthetic, natural based dye-sensitized solar cells. *Materials Science for Energy Technologies* 2020, 3, 183-192. https://doi.org/10.1016/j.mset.2019.09.010
30. Height, M.J.; Pratsinis, S.E.; Mekasuwandumrong, O.; Praserthdam, P. Ag-ZnO catalysts for UV-photodegradation of methylene blue. *Applied Catalysis B: Environmental* 2006, 63(3-4), 305-312. https://doi.org/10.1016/j.apcatb.2005.10.018
31. Loka, C.; Lee, K.-S. Enhanced visible-light-driven photocatalysis of $Ag/Ag_2O/ZnO$ nanocomposite heterostructures. *Nanomaterials* 2022, 12(15), 2528. https://doi.org/10.3390/nano12152528
32. Nosaka, Y.; Nosaka, A. Y. Generation and detection of reactive oxygen species in photocatalysis. *Chemical Reviews* 2017, 117(17), 11302–11336. https://doi.org/10.1021/acs.chemrev.7b00161
33. Houas, A.; Lachheb, H.; Ksibi, M.; Elaloui, E.; Guillard, C.; Herrmann, J.-M. Photocatalytic degradation pathway of methylene blue in water. *Applied Catalysis B: Environmental* 2001, 31(2), 145–157. https://doi.org/10.1016/S0926-3373(00)00276-9
34. Behnajady, M.A.; Modirshahla, N.; Hamzavi, R. Kinetic study on photocatalytic degradation of C.I. Acid Yellow 23 by ZnO photocatalyst. *Journal of Hazardous Materials* 2006, 133(1–3), 226–232. https://doi.org/10.1016/j.jhazmat.2005.10.022